Giant Photo-induced Chirality in Thin Film Ge$_2$Sb$_2$Te$_5$

Janaki Shanmugam*, Konstantin B. Borisenko*, Andrew Luers, Paul Ewart, Priyav Shah,

Benjamin A. O. Williams, Christopher Craig, Daniel W. Hewak, Rohanah Hussain, Tamás

Jávorfi, Giuliano Siligardi, Michel Bosman and Angus I. Kirkland

Dr. J. Shanmugam

Department of Materials, University of Oxford, Parks Road, Oxford, OX1 3PH, United

Kingdom; Institute of Materials Research and Engineering, Agency for Science, Technology

and Research, 138634 Singapore, E-mail: janaki_shanmugam@imre.a-star.edu.sg

Dr. K. B. Borisenko

Department of Materials, University of Oxford, Parks Road, Oxford, OX1 3PH, United

Kingdom, Email: konstantin.borisenko@gmail.com

Dr. A. Luers, Prof. P. Ewart

Clarendon Laboratory, Department of Physics, University of Oxford, Parks Road, Oxford,

OX1 3PU, United Kingdom

P. Shah, Prof. B. A. O. Williams

Department of Engineering Sciences, University of Oxford, Parks Road, Oxford, OX1 3PJ,

United Kingdom

C. Craig, Prof. D. W. Hewak

Optoelectronics Research Centre, University of Southampton, Southampton, SO17 1BJ,

United Kingdom

Dr. R. Hussain, Dr. T. Jávorfi, Dr. G. Siligardi

Diamond Light Source, Harwell Science and Innovation Campus, Didcot, Oxfordshire OX11

0DE, United Kingdom

Dr. M. Bosman

Department of Materials Science and Engineering, National University of Singapore, 9

Engineering Drive 1, 117575 Singapore; Institute of Materials Research and Engineering,

Agency for Science, Technology and Research, 138634 Singapore

Prof. A. I. Kirkland

Department of Materials, University of Oxford, Parks Road, Oxford, OX1 3PH, United

Kingdom

Abstract

Induction, tuning or amplification of chirality in various classes of materials and probing their

chiral response is a subject of growing research. Here, we report a large chiral signal that is

rapidly imprinted in achiral amorphous $Ge_2Sb_2Te_5$ (GST) thin films measured using

synchrotron circular dichroism spectroscopy. The chirality is induced by illuminating the

films with pulsed circularly polarized (chiral) laser light for less than 2 microseconds in total.

The effects of laser fluence and film thickness on the chiral response are reported. Correlation

of the optical results with structural studies by electron diffraction and model simulations

suggests that alignment of re-amorphized fragments in the crystallized film along the electric

field vector of the light forms the centers that are responsible for the observed chirality. These

results suggest opportunities for practical applications of this phenomenon and provide

avenues for further studies of chirality induction in materials with impact in a wide range of

disciplines.

1. Introduction

Chirality in materials underpins a variety of important properties and applications (e.g.

magnetic circular dichroism, [1] chiral skyrmions, [2] chiral metamaterials [3] and the

preparation of stable enantiomerically pure compounds in pharmaceuticals). [4] Chiral structures are known to exhibit circular dichroism (differential absorption of differently circularly polarized or chiral light). Transformation of originally achiral materials by chiral light illumination is an attractive processing option. [5–7] However, this has only been achieved using exposures ranging from minutes up to tens of hours.

$Ge_2Sb_2Te_5$ (GST) is an important functional material displaying a rapid reversible phase transition between amorphous and crystalline states, which has been utilized in optical and electronic data storage [8,9] and has been used more recently in non-volatile universal memory and optoelectronics applications. [10–13]

We have previously reported [14] optically-induced phase transitions at nanosecond time scales resulting in chirality in pure and N-doped GST thin films measured using circular dichroism (CD) spectroscopy. However, the small magnitude of the signal achieved in that study made applications of the phenomenon (e.g. in chiroptical switches or sensors) impractical.

We report here a large chiral signal induced in achiral amorphous GST films by illumination with circularly polarized light (λ= 532nm) in a fraction of the time previously reported (in the order of seconds). The effects of film thickness and laser fluence on the CD signal are also described. The increase in signal from the previous study can be attributed to the use of thicker GST films on a different substrate and larger laser fluence using an optimized laser irradiation setup. CD spectroscopy measurements are also correlated with structural characterization and model simulations to provide an insight into the origin of the observed CD signal in the irradiated GST films.

2. Results

The results of CD spectroscopy indicated a considerable mirror-symmetric signal that was dependent on the handedness of the circularly polarized laser light (CPL) used to irradiate

a region in the GST film (Figure 1), whereas linearly polarized light (LPL) caused a signal with negligible magnitude. We therefore focus our discussion on the results from CPL-irradiated films.

The fluence or energy density used to irradiate regions of the GST thin films was found to have an impact on the CD signal intensity and the wavelength at which the maximum signal was measured. Initially, an increase in the laser power used to induce transformation in the sample resulted in an increase in the maximum signal intensity (Figure 1a and 1b), where the largest CD signal of 1160 millidegrees was measured from a region of a 55nm thick GST film irradiated with 15.5 mJ/cm^2 (L-CPL). However, a decrease in the signal was observed with a further increase in fluence to 19 mJ/cm^2 (Figure 1c).

These changes in CD signal as a function of laser fluence can be correlated to changes in the morphology of the irradiated spots. Our preliminary investigations [14] on films irradiated at low laser fluence (<7 mJ/cm^2) showed brighter reflective crystalline regions without detectable changes in the film surface. Increasing the laser fluence to 8-9 mJ/cm^2 resulted in modification of the film surface, with breaking and possible local melting of the film at the center of the irradiated region leading to the formation of droplet-like surface features (Figure 1f).

Lateral dissipation of heat allows this melt region to grow with increasing laser fluence, and with a fluence over 10 mJ/cm^2, the observed surface features are attributed to a melt-quench transition from a crystalline back to an amorphous state, while retaining a brighter peripheral crystalline ring. Still higher fluence irradiation leads to decrease of this melt region as material is ablated from the center of the irradiated spot. These observations of laser-induced changes in the material are consistent with the Gaussian intensity profile of the laser beam and are similar to core-ring structures patterned by laser lithography. [15]

If the chiral structures are generated in the melt-quenched and re-amorphized region, the increase in CD signal can, therefore, be associated with an increase in the amount of chiral

structures in the film as the modified area grows with initially increasing laser fluence. The observed decrease in signal intensity with a further increase in laser fluence is consistent with ablation of material from the center of the irradiated regions, leading to a decrease in the amount of chiral structures in the modified film. Similarly, the larger signal intensity exhibited by 55nm thick GST films as compared to 35nm films (Figure 1d) for all laser fluence studied can be attributed to an increase in the amount of chiral structures.

An increase in film thickness, as well as laser fluence, also gave rise to a red shift in the peak CD signal intensity. This shift in CPL absorption maxima to longer wavelengths suggests a dominance of lower energy excitations when the CPL interacts with chiral structures in structurally modified regions. The change in the absorption maximum can be attributed to changes in the resonant bonding in crystalline phase change material [16] and associated electron delocalization leading to the red shift [17] observed in the laser-irradiated GST films.

The modified surface features (Figure 1f) were cross-sectioned for further TEM/STEM analysis to examine the structure of possible chiral centers. Energy dispersive X-ray (EDX) compositional analysis of these features shows a Sb/Te-rich phase within the surface features, with a Ge-rich phase located at the periphery (Figure 1g). This crystallization-induced or solidification-induced segregation, [18] that occurs when different phases solidify at different temperatures, is significant as this will increase the anisotropy of the material and contribute to the CD signal.

A possible origin of the chiral centers and consequently the mechanism of photo-induced chirality was investigated using electron diffraction to provide a structural analysis of the transformed films compared to the original amorphous state. Figure 2 shows Reduced Density Functions (RDF) extracted from electron diffraction data obtained from a reference 20nm thick amorphous GST film (floated from a NaCl substrate) and a set of cross-sectioned irradiated film regions that produced the highest CD signal intensities (55nm thick GST film

on a LiF substrate irradiated with 15.5 mJ/cm^2 fluence). These were recorded using quasi-parallel STEM probe illumination, together with conventional selected area electron diffraction (SAED) reference data taken from amorphous and crystallized regions of a plan-view film. Examples of the diffraction patterns are given in the supporting information (Figures S6 and S7). A legend key to the RDF curve labels is given in Figure 2d.

RDF curves obtained from as deposited amorphous films over two different illumination areas (1.6μm effective SAED aperture diameter versus 10nm quasi-parallel STEM probe diameter) are globally similar (Figure 2a), with peak positions at r_1 = 0.275±0.002nm, r_2 = 0.420±0.004 nm and r_3 = 0.635±0.004 nm. This confirms that the structural data obtained from RDF measurements is independent of the beam size used in different experiments. The observed peak positions are also in agreement with values found in previous investigations, [19–21] where r_1 has been reported to be between 0.267nm and 0.270nm, r_2 between 0.401nm and 0.414nm, and r_3 between 0.620nm and 0.666nm. Variations in these values may originate from differences in sample preparation in different experiments, the presence of crystallites (as observed by electron diffraction in the present study), electron beam-induced modifications, surface contamination or native oxidation.

When the original amorphous GST film is crystallized under electron beam irradiation, clear differences in the RDF curves are observed. In particular, the RDF curve from a polycrystalline sample ('SAED_crystalline' in Figure 2a) exhibits an additional peak at ~0.53nm (r_c) and splitting of the r_3 peak. The first three peak positions (r_1, r_2 and r_c) are close to those expected for a cubic rock salt structure, suggesting that the presence of a crystalline fraction in the GST film will shift the peaks toward their ideal crystalline values.

However, the RDF curves obtained from laser-irradiated regions (Figure 2b, 2c) show closer similarity to the amorphous RDF than to the polycrystalline RDF. The broadening and splitting of the peaks, as well as the variation in the r_2 and r_3 peak shoulders, indicate greater

local disorder and a larger spread of nearest and next-nearest neighbor distances in the irradiated regions compared to the as-deposited films.

Our data indicates that the irradiated film regions have been initially crystallized and then partially re-amorphized by the laser light. Some melt-quenched regions appear to retain crystalline fragments, as suggested by the proximity of local maxima (at ~0.52nm in the 'STEM_RCPL_1' and 'STEM_LCPL_2' RDF curves in Figure 2b and 2c respectively) to the characteristic crystalline r_c peak at 0.521nm and the presence of crystalline speckle in the electron diffraction patterns acquired from the interior of the modified surface features (Figure S7d). A local maximum is also observed at ~0.52nm in the 'STEM_Amorphous' RDF curve (Figure 2a), which shows longer interatomic distances than those in other reported studies of amorphous GST [19–21] possibly due to the presence of nano-crystallites.

We also studied the influence of an electric field applied perpendicular to thin film models of GST in molecular dynamics simulations using density functional theory. The model annealed with an electric field exhibited a lower total number of bonds than the model simulated without a field, suggesting a decrease in density and an increase in Ge-Te and Sb-Te bonds at the expense of homopolar bonds (Figure 3a). This was also reflected in the distribution of related bond angles (Figure 3b).

The annealing process employed in the liquid quench simulations resulted in cross-linked structures in both models, including predominantly 4-membered rings and smaller numbers of 3 and 5-membered rings (Figure 3c) and 6-membered rings in the model quenched under an electric field. However, the extent of cross-linking is reduced in the model with an applied electric field due to a decrease in homonuclear Sb-Sb and Te-Te bonds, resulting in an increase in ring structures and chains formed with Ge-Te and Sb-Te bonds.

Comparison of the distribution of bond angles with respect to the electric field vector direction (Figure 3d, 3e) in both thin film models also suggests preferential alignment of Ge-Te and Sb-Te bonds perpendicular to the field vector. However, no phase segregation is

observed in the model simulated under the electric field, due to the extremely short timescale used in the simulations (8ps) compared to a single laser pulse duration of 8ns and total experimental irradiation time of 1.6μs.

Overall, our simulations indicate that the electric field arising from the laser pulse has a considerable effect on the alignment of bonds in the films during melt quench.

3. Discussion

Absorption spectra and dissymmetry factors (CD values normalized to absorption) can be reported as a measure of optical activity that is independent of the amount of material probed. A comparison of absorption spectra (Figure S8 in supplementary information) from film regions before and after irradiation shows a decrease in absorbance of the irradiated regions at wavelengths beyond 200nm. This, in addition to the decrease in absorbance with increasing fluence, is consistent with the observed evaporation of part of the irradiated material. However, there is only small difference between the spectra acquired from regions irradiated with different polarization (whether CPL or LPL). Given the small changes in the absorption spectra of various irradiated regions of the same GST film, and with the only difference between them being the polarization of laser irradiation, only CD values are discussed here.

From the results of diffraction studies, the r_1 peak in the 'STEM_LCPL' RDF curves (Figure 2c) occurs at up to 0.015nm shorter distance than that observed in the 'STEM_RCPL' (Figure 2b) and 'STEM_Amorphous' (Figure 2a) RDF curves and is closer to previously reported values [19–21]. This shift of the r_1 peak position towards shorter distances and differences in the r_1/r_2 peak ratio are attributed to a shortening of the dominant Ge-Te and Sb-Te bonds due to increased electron localization, [20] suggesting more amorphous character in the L-CPL-irradiated regions than in the probed regions of the R-CPL-illuminated spot. This difference is intriguing because it mirrors the consistently larger CD signal observed for L-

CPL-illuminated areas than for those illuminated with R-CPL in the series of materials examined in the present study. However, the shift of the r_1 peak position may also be attributed to the variations in local order across the whole spot which is locally sampled in the diffraction analyses on the scale of the probe size used (about 10nm) within a total lamella of approximately 10μm long.

In support of our hypothesis that light affects phase transitions in other ways than thermally, recent experiments have attributed photo-induced phase transitions to electronic excitation at sub-ns timescales. [22–24] It has also been reported that photo-induced crystallization of amorphous selenium films is polarization dependent. [25] While an alternative thermal mechanism involving the preferential growth of Se crystallites oriented to linearly-polarized light has been proposed, [26] photo-induced melting of both amorphous and crystalline Se films [27] as well as amorphization of As_2S_3 [28] have been described as athermal phenomena. Amorphous GST alloy films excited with linearly-polarized fs laser pulses have displayed similar optical anisotropy following crystallization. [29] A recent report on asymmetric laser desorption of enantiomers from a racemic mixture exposed to CPL also supports non-thermal processes in CPL irradiation. [30]

The preferential alignment of the dominant Ge-Te and Sb-Te bonds perpendicular to the applied electric field observed in simulations, even within short timescale of 8ps, implies that effects of a rotating field vector (in the case of circularly polarized light) can lead to similar alignment and consequently the formation of chiral centers. This effect is expected to be enhanced in the repeated pulses; as light propagates through the film, the rotation of the field vector amounts to about 24 degrees for 532nm light and film thickness of 35nm.

Taking these observations into account, we propose the following overall mechanism for the photo-induced chirality that is observed in GST films. The intense laser light initially crystallizes and then partially re-amorphizes the as-deposited amorphous GST film. During this process the re-amorphized fragments of the crystalline film are aligned by the electric

field vector of the light to form chiral centers. The presence of asymmetric chain cross-linking and ring structures in the simulated models support the presence of motifs in melt-quenched material that may contribute to the formation of chiral centers. Moreover, if these chiral structures are responsible for the CD signal intensity observed, an increased amount of chiral structures would then result in greater CPL absorption and a higher CD signal intensity, as observed for thicker films and films irradiated with higher fluence.

4. Experimental section

Thin film growth: $Ge_2Sb_2Te_5$ amorphous films 35±3nm and 55±3nm thick were deposited by magnetron radio frequency (RF) sputtering using a $Ge_2Sb_2Te_5$ target in an argon atmosphere onto 25mm diameter LiF (2mm thick) disk substrates supported on a rotating stage. The substrate was chosen for its optical transparency between 180nm and 600nm, making it suitable for subsequent optical measurements in the same wavelength range. A 20nm film was also grown on a 10x10mm NaCl (1mm thick) substrate for electron microscopy studies. All deposited film thicknesses were measured using a depth profiler.

Laser irradiation: Phase transitions in the as-deposited amorphous films on LiF substrates were induced using nanosecond pulses (8ns FWHM (full width half maximum) pulse width, 10 Hz repetition rate) of left (L-) or right (R-) circularly polarized light (CPL) generated using a Nd:YAG laser at a wavelength of 532nm (second harmonic). A linear polarizer (Glan-Taylor prism) was used to ensure a 100% plane polarized wave incident on a quarter wave plate (rotated at 45° with respect to the fast or slow axes of the quarter wave plate). The laser beam was subsequently switched between left and right-handed circularly polarized states by rotating the quarter-wave plate by 90°. Linearly polarized light (LPL) was generated by removing the quarter wave plate from the beam path. The samples were mounted with the film facing the beam at 90° angle of incidence and were irradiated with fluence of 10.3 mJ/cm^2, 15.5 mJ/cm^2 and 19 mJ/cm^2 for each polarization. The total exposure duration was standardized at 20s, equivalent to about 1.6μs of laser illumination.

Synchrotron Circular Dichroism (CD) Spectroscopy: CD spectra were measured from laser-irradiated areas (approximately 2mm in diameter) and amorphous reference regions in the GST films using a highly collimated beam with a cross-section of about 0.6mm in diameter, generated by synchrotron radiation at the circular dichroism beamline B23 at the Diamond Light Source in Oxfordshire, UK.

A MgCl$_2$ Rochon polarizing prism was installed in the module B spectrometer before the fused silica photoelastic modulator (PEM), which acted as a quarter-wave plate. The Rochon prism splits the incident elliptically-polarized synchrotron radiation into two orthogonal linearly polarized beams and rotation of the prism between two orthogonal positions effectively rotates the incident light polarization on the sample by 90° with no change in the sample position. Summation of the two spectra recorded at both Rochon prism positions provides an estimate of the contribution of linear effects to the observed CD spectra,

while the difference between the two spectra is effectively a double CD signal as detailed in our previous work. [14]

The spectra were recorded in single-beam mode using two Rochon prism rotations in the UV-visible spectral range, with 5nm steps between 180nm and 600nm and averaged over four scans with an integration time of 1s at each data point. Doubled CD spectra from laser-irradiated regions were normalized against averaged spectra from amorphous regions (Figure S2) by subtracting the amorphous spectral values from laser-irradiated spectral values at corresponding wavelengths. This allows the effects of various experimental factors on the CD signal from different samples and irradiations to be compared in a robust manner. The errors in the spectra were estimated as a standard deviation computed from repeated collections, which were then propagated in doubled CD spectra by calculating the square root of the sum of squared standard deviations from spectra obtained from two orthogonal positions of the Rochon prism.

Sample preparation for electron microscopy: 20nm thick amorphous GST thin films deposited on NaCl substrates were floated off in water and picked up directly onto 3mm mesh copper TEM grids coated with lacey carbon. A dual-beam system (FEI Helios NanoLab 460S) was used to prepare electron-transparent cross-section lamellae from laser-irradiated film regions on a LiF substrate (coated with protective capping layers of gold and/or carbon) using a standard lift-out procedure, including ion milling at 30kV, followed by final low voltage milling at 5kV and 2kV.

Transmission electron microscopy (TEM): Electron diffraction data was obtained using a quasi-parallel STEM probe (convergence semi-angle of 0.34mrad and beam diameter of less than 10nm) in a FEI Titan microscope at 200kV. Diffraction patterns were recorded using a Gatan OneView camera using the full 4K x 4K pixel array and summed over at least 10 non-overlapping acquisitions of up to 60s each to improve the signal-to-noise ratio. Selected area electron diffraction (SAED) patterns were recorded using a JEOL JEM-2100 at 200kV using an aperture with effective illumination diameter of 1.6μm. EDX compositional analysis was performed with a beam current of 1nA on the Titan at 200kV using an EDAX Si(Li) detector and spectra were collected up to 20keV with an energy resolution of 134eV and a collection solid angle ≤ 0.3sr.

RDF analysis: Reduced density functions (RDF) were extracted from azimuthally averaged intensities in the electron diffraction patterns recorded from plan-view amorphous GST films and laser-irradiated cross-sectional specimens using eRDF Analyser. [31] The scattering vector q was calibrated using diffraction data recorded from polycrystalline aluminum films or gold layers in the cross-sectional specimens under the same recording conditions used for the GST specimens. Diffraction data with q up to 155nm^{-1} were used.

MD simulations: Density Functional Theory (DFT) Molecular Dynamics (MD) simulations of a model of GST were performed using the CASTEP code. [32] A small model of GST was constructed by random dense packing of 108 atoms in a cubic cell with lattice parameter (a=1.515nm) corresponding to a density of 5.88 g/cm^3. A liquid quench simulation of this model using a canonical (constant NVT) ensemble starting from 2000K and involving gradual cooling to 300K in 200K steps was performed. The resulting model was placed in a supercell with 3nm vacuum layer along the *z* dimension to prepare a thin film model, which was then heated at 800K for 2ps, gradually cooled to 400K in steps of 200K (2ps per step), and equilibrated at 300K for a further 2ps.

Two further simulations were carried out using similar quench rates and a total simulation time of 8ps as above, both with and without the influence of an electric field (magnitude of 7.6 x 10^6 V/m as estimated from the laser irradiation parameters) applied perpendicular to the film (i.e. along the *z* direction). The MD simulations were performed using the Perdew-Burke-Ernzerhof (PBE) functional and a 200eV pseudopotential energy cut-off, where the energy was sampled at the gamma point of the Brillouin zone only. DFT energy optimization of the quenched thin film models were performed with full geometry relaxation under rigid periodic boundary conditions, using a pseudopotential energy cut-off at 300eV.

References

[1]   A. Rogalev, K. Ollefs, F. Wilhelm, in *X-Ray Absorpt. X-Ray Emiss. Spectrosc.* (Eds.: J.A. Van Bokhoven, C. Lamberti), John Wiley & Sons, Ltd, Chichester, UK, **2016**, pp. 671–694.

[2]   R. Wiesendanger, *Nat. Rev. Mater.* **2016**, *1*, 16044.

[3]   S. Yoo, Q.-H. Park, *Nanophotonics* **2019**, *8*, 249.

[4]   W. H. Brooks, W. C. Guida, K. G. Daniel, *Curr. Top. Med. Chem.* **2011**, *11*, 760.

[5]   R. J. Cave, *Science* **2009**, *323*, 1435.

[6]   J. Yeom, B. Yeom, H. Chan, K. W. Smith, S. Dominguez-Medina, J. H. Bahng, G. Zhao, W.-S. Chang, S.-J. Chang, A. Chuvilin, D. Melnikau, A. L. Rogach, P. Zhang, S. Link, P. Král, N. A. Kotov, *Nat. Mater.* **2015**, *14*, 66.

[7]   Y. Wang, T. Harada, L. Q. Phuong, Y. Kanemitsu, T. Nakano, *Macromolecules* **2018**, *51*, 6865.

[8]   N. Yamada, E. Ohno, K. Nishiuchi, N. Akahira, M. Takao, *J. Appl. Phys.* **1991**, *69*,

2849.

[9]   M. Gill, T. Lowrey, J. Park, in *2002 IEEE Int. Solid-State Circuits Conf. Dig. Tech. Pap. (Cat. No.02CH37315)*, **2002**, pp. 202–459 vol.1.

[10]   Y. Lu, M. Stegmaier, P. Nukala, M. A. Giambra, S. Ferrari, A. Busacca, W. H. P. Pernice, R. Agarwal, *Nano Lett.* **2017**, *17*, 150.

[11]   B. Gholipour, A. Karvounis, J. Yin, C. Soci, K. F. MacDonald, N. I. Zheludev, *NPG Asia Mater.* **2018**, *10*, 533.

[12]   W. Zhang, R. Mazzarello, M. Wuttig, E. Ma, *Nat. Rev. Mater.* **2019**, *4*, 150.

[13]   P. Guo, M. A. Sarangan, I. Agha, *Appl. Sci.* **2019**, *9*, DOI 10.3390/app9030530.

[14]   K. B. Borisenko, J. Shanmugam, B. A. O. Williams, P. Ewart, B. Gholipour, D. W. Hewak, R. Hussain, T. Javorfi, G. Siligardi, A. I. Kirkland, *Sci. Rep.* **2015**, *5*, 8770.

[15]   C. H. Chu, C. Da Shiue, H. W. Cheng, M. L. Tseng, H.-P. Chiang, M. Mansuripur, D. P. Tsai, *Opt. Express* **2010**, *18*, 18383.

[16]   K. Shportko, S. Kremers, M. Woda, D. Lencer, J. Robertson, M. Wuttig, *Nat. Mater.* **2008**, *7*, 653.

[17]   H. W. Ho, K. Bai, W. D. Song, T. L. Tan, R. Zhao, C. M. Ng, L. Wang, *Acta Mater.* **2013**, *61*, 1757.

[18]   A. Debunne, K. Virwani, A. Padilla, G. W. Burr, A. J. Kellock, V. R. Deline, R. M. Shelby, B. Jackson, *J. Electrochem. Soc.* **2011**, *158*, H965.

[19]   C. Lang, S. A. Song, D. Nguyen-Manh, D. J. H. Cockayne, *Phys. Rev. B* **2007**, *76*, 054101.

[20]   K. B. Borisenko, Y. Chen, S. A. Song, D. Nguyen-Manh, D. J. H. Cockayne, *J. Non. Cryst. Solids* **2009**, *355*, 2122.

[21]   G.-S. Park, J.-H. Kwon, M. Kim, H. R. Yoon, W. Jo, T. K. Kim, J.-M. Zuo, Y. Khang, *J. Appl. Phys.* **2007**, *102*, 013524.

[22]   J. Tominaga, L. Bolotov, *Appl. Phys. Express* **2018**, *12*, 15504.

[23]   L. Waldecker, T. A. Miller, M. Rudé, R. Bertoni, J. Osmond, V. Pruneri, R. E. Simpson, R. Ernstorfer, S. Wall, *Nat. Mater.* **2015**, *14*, 991.

[24]   T. A. Miller, M. Rudé, V. Pruneri, S. Wall, *Phys. Rev. B* **2016**, *94*, 024301.

[25]   V. K. Tikhomirov, P. Hertogen, C. Glorieux, G. J. Adriaenssens, *Phys. status solidi* **1997**, *162*, R1.

[26]   V. V. Poborchii, A. V. Kolobov, K. Tanaka, *Appl. Phys. Lett.* **1998**, *72*, 1167.

[27]   V. V. Poborchii, A. V. Kolobov, K. Tanaka, *Appl. Phys. Lett.* **1999**, *74*, 215.

[28]   M. Frumar, A. P. Firth, A. E. Owen, *J. Non. Cryst. Solids* **1995**, *192–193*, 447.

[29]   N. Kitamura, Y. Katsumata, T. Morita, T. Hira, T. Saiki, in *11th Eur. Phase Chang. Ovonics Sci. Symp.*, Tampere, Finland, **2012**.

[30]   F. Mortaheb, K. Oberhofer, J. Riemensberger, F. Ristow, R. Kienberger, U. Heiz, H. Iglev, A. Kartouzian, *Angew. Chemie Int. Ed.* **2019**.

[31]   J. Shanmugam, K. B. Borisenko, Y.-J. Chou, A. I. Kirkland, *SoftwareX* **2017**, *6*, 185.

[32]   S. J. Clark, M. D. Segall, C. J. Pickard, P. J. Hasnip, M. I. J. Probert, K. Refson, M. C. Payne, *Zeitschrift für Krist. - Cryst. Mater.* **2005**, *220*, 567.
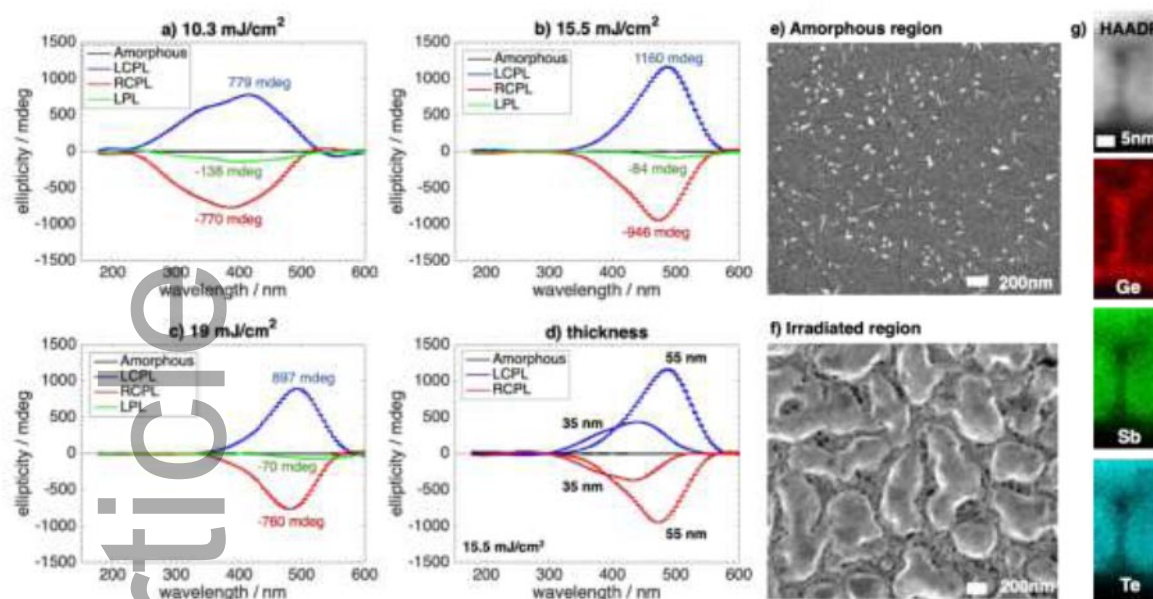
Figure 1. (a-c) Effect of laser fluence on CD signal; Normalized doubled CD spectra measured from regions of a 55nm thick GST film irradiated at (a) 10.3 mJ/cm^2, (b) 15.5 mJ/cm^2 and (c) 19 mJ/cm^2.

(d) Effect of film thickness; Normalized doubled CD spectra from irradiated regions of 35nm and 55nm thick GST films irradiated at 15.5mJ/cm^2.

(e-f) SEM secondary electron images of (e) the surface of an amorphous region (white specks are surface contaminants) of a 55nm thick GST film and (f) the central region of a laser-irradiated spot (at a fluence of 15.5mJ/cm^2). (g) HAADF STEM image of a cross-sectioned surface feature and corresponding elemental maps of integrated EDX signal intensities of Ge, Sb and Te.
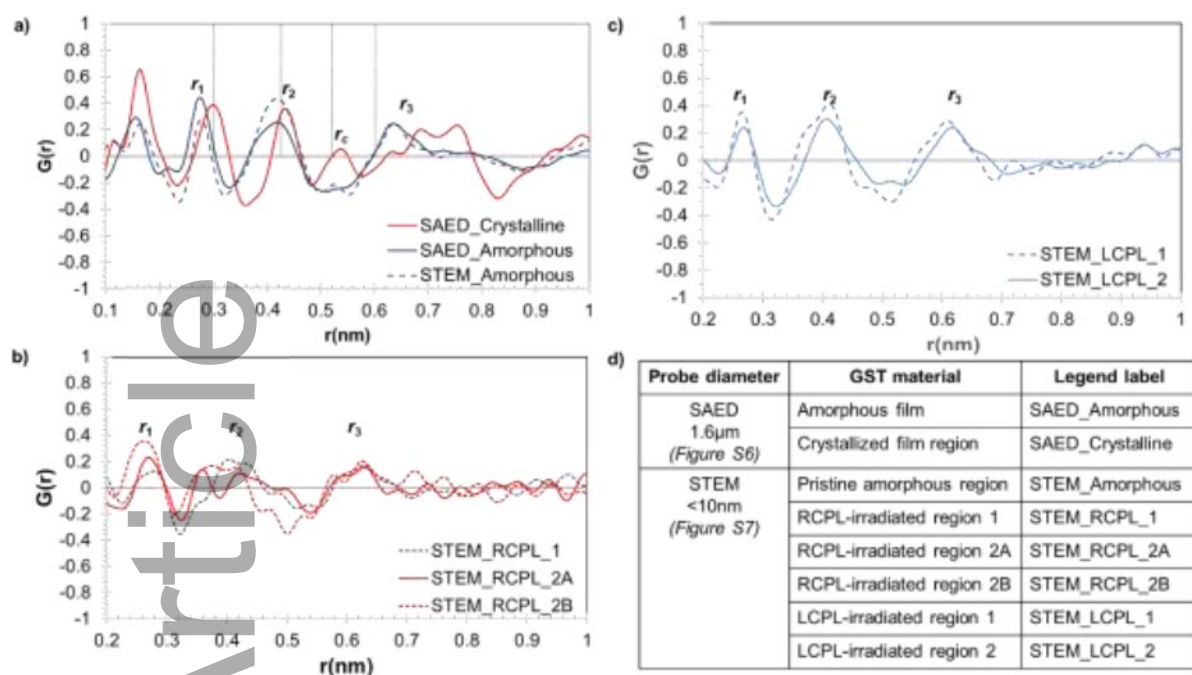
Figure 2. (a) RDF curves obtained from selected area diffraction (SAED) and quasi-parallel STEM probe diffraction data of amorphous and crystallized regions of 20 nm GST thin films. (b, c) Quasi-parallel STEM probe diffraction data of irradiated regions of a 55nm thick GST film on a LiF substrate (irradiated with b) R-CPL and c) L-CPL and a fluence of 15.5 mJ/cm^2). (d) Legend key to RDF curve labels used in (a – c). The vertical lines in (a) represent the first four interatomic distances for a cubic rock salt structure (with lattice constant a = 0.602nm); r_i refers to the i-th peak position, where r_1 is the nearest-neighbor distance; r_c refers to the characteristic peak in crystalline GST.
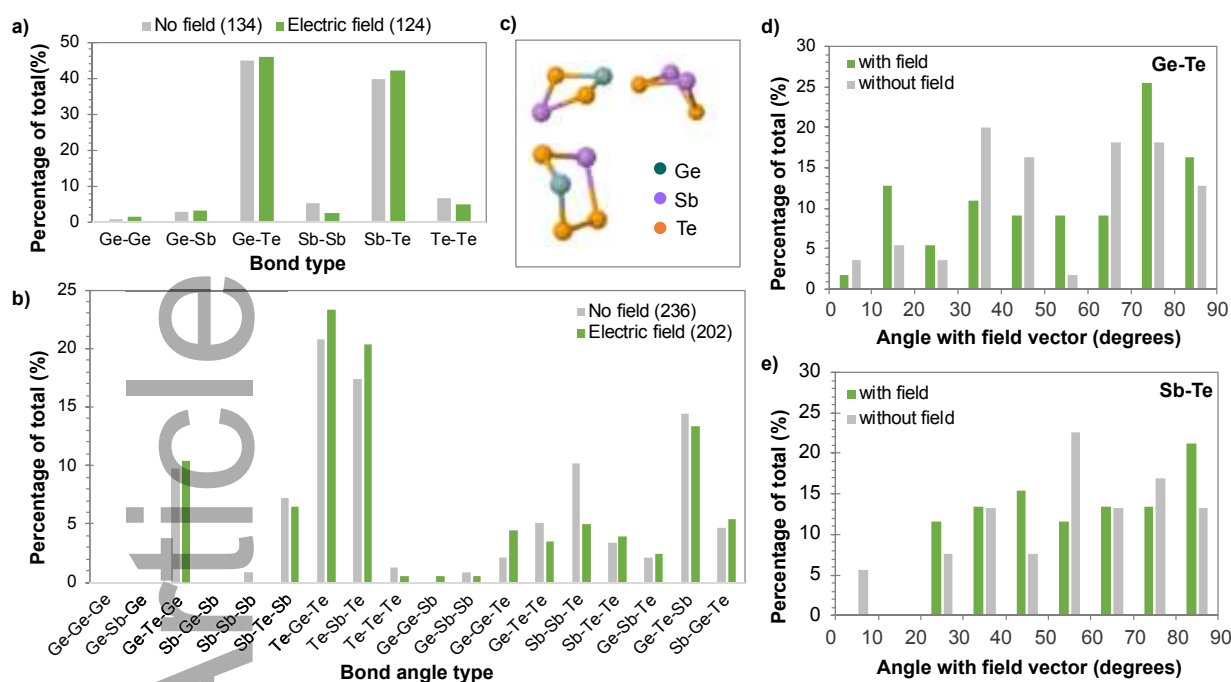
Figure 3. Results from the MD and DFT simulations. (a) Bond type and (b) bond angle type distributions in the models annealed with (green) and without (grey) an applied electric field, expressed as percentages of the total number of bonds (in brackets). (c) Examples of closed ring structures present in GST.

Distribution of (d) Ge-Te and (e) Sb-Te bond angles with respect to the electric field unit vector in the thin film models annealed with and without the field. The model with an applied field exhibits an increase in Ge-Te bonds perpendicular (70°-90°) to the vector and a decrease in Sb-Te bonds parallel (0°-20°) to the vector compared to the model without a field.

ToC

A giant circular dichroism signal of different chirality can be rapidly imprinted in amorphous $Ge_2Sb_2Te_5$ (GST) thin films by illuminating the films with pulsed circularly polarized (chiral) laser light. The large signal opens opportunities for practical applications of this phenomenon.

Keyword photo-induced chirality

J. Shanmugam*, K. B. Borisenko*, A. Luers, P. Ewart, P. Shah, B. A. O. Williams, C. Craig, D. W. Hewak, R. Hussain, T. Jávorfi, G. Siligardi, M. Bosman and A. I. Kirkland

Giant Photo-induced Chirality in Thin Film Ge$_2$Sb$_2$Te$_5$

ToC figure